A new angle into time-resolved photoacoustic spectroscopy: A layered prism cell increases experimental flexibility

Tom Autrey,[a] Nancy S. Foster, Kim Klepzig, James E. Amonette, and John L. Daschbach
Pacific Northwest National Laboratory, Post Office Box 999, Richland, Washington 99352

(Received 27 January 1998; accepted for publication 10 March 1998)

A new pulsed photoacoustic calorimetry cell that uses transmission of light through a pair of dovetail prisms is discussed. The layered prism cell (LPC) combines the enhanced time-resolution capabilities of the ''layered'' front-face irradiation geometry with the zero-background and broadband flexibility of the classical cuvette geometry. This work provides a phenomenological description of photoinduced pressure changes to yield an analytical expression to calculate the magnitude of the photoinduced acoustic pressure wave in a series of solvents. The mechanical to electrical conversion efficiency for an ultrasonic transducer coupled to the LPC is presented to provide a comparison of the experimentally observed photoinduced acoustic signal amplitudes to the empirically calculated acoustic signal amplitudes. An analysis of the background signals due to absorption and electrostriction of the media provides insight into the issues of sensitivity and limitations of pulsed photoacoustic experiments. The LPC provides several benefits to increase the flexibility of the photoacoustic spectroscopy: (1) greater sensitivity, (2) enhanced time resolution, and (3) the ability to obtain kinetic data in complex solvent mixtures. Under optically dilute conditions in the layered cell geometry, the acoustic transient time, τa, approaches zero because the photoinduced acoustic wave homogeneously expands against the walls of the photoacoustic cell. To demonstrate the unique capabilities of the LPC, rates of hydrogen abstraction by *tert*-butoxyl radical from solvent mixtures containing ethyl and methyl alcohol are presented. © *1998 American Institute of Physics.* [S0034-6748(98)01106-X]

I. INTRODUCTION

Photoacoustic calorimetry (PAC) has been demonstrated to be a versatile experimental technique capable of providing both kinetic and thermochemical information for short-lived reactive intermediates.[1–15] PAC provides the unique ability to study the reactions of reactive intermediates that have little or no absorbance to be monitored by time-resolved transient absorption methods or electron spin resonance methods because the photoacoustic signal is a measure of the time-dependent release of heat from the reactions of photogenerated reactive intermediates.

Two different experimental geometries are commonly used in pulsed PAC: (1) the traditional cuvette cell (CC)[14,16–19] with the piezoelectric detector acoustically coupled parallel to incident excitation beam, and (2) the more recently developed front-face irradiation[20,21] or layered reflector cell[22,23] (LRC), with the piezoelectric detector acoustically coupled to a dielectric reflector normal to the incident excitation beam. The cuvette geometry is still the preferred experimental choice to collect PA absorption spectra[24–27] due to the ability to collect data over the entire UV-visible and near-IR range and for the analysis of weakly absorbing solutions[26,28,29] due to the inherent zero background. Recently, significant improvements to the CC geometry have been recognized by using a planar beam of light[30,31] (as opposed to the cylindrical beam)[32] for the excitation source. However, even with the improvements to the CC geometry, the LRC undoubtedly provides both enhanced time resolution and greater sensitivity.[33,34] In general, the PA spectroscopist faces a dilemma, does the experiment require broadband detectability or analysis of optically dilute solutions dictating use of the cuvette design, or does the experiment require faster time resolution dictating use of the layered PA geometry.

In this article, a new experimental PA cell geometry that uses a pair of prisms is described. This novel layered prism cell (LPC) design increases the PA spectroscopist's flexibility by combining the enhanced time resolution provided by the layered cell with the broadband tunability and ''zero'' background benefits of the cuvette cell. The work covered in this review examines the fundamental properties of photoinduced acoustic pressure waves arising from absorption and electrostriction to provide a basis for detailed comparison of the LPC with previous photoacoustic cell designs. This approach yields a mechanism to discuss the benefits and the limitations of the various PA cell geometries. The result is a new PA cell that can provide an experimental approach to measure the rates of reactions on a nanosecond time scale in complex solvent mixtures under optically dilute conditions. To demonstrate the unique kinetic abilities of the LPC, the rates of hydrogen transfer from a complex solvent mixture to a reactive intermediate, *tert*-butoxyl radical, are measured.

[a]Electronic mail: red@pnl.gov

 © 1998 American Institute of Physics

Downloaded 06 May 2003 to 198.128.86.151. Redistribution subject to AIP license or copyright, see http://ojps.aip.org/rsio/rsicr.jsp

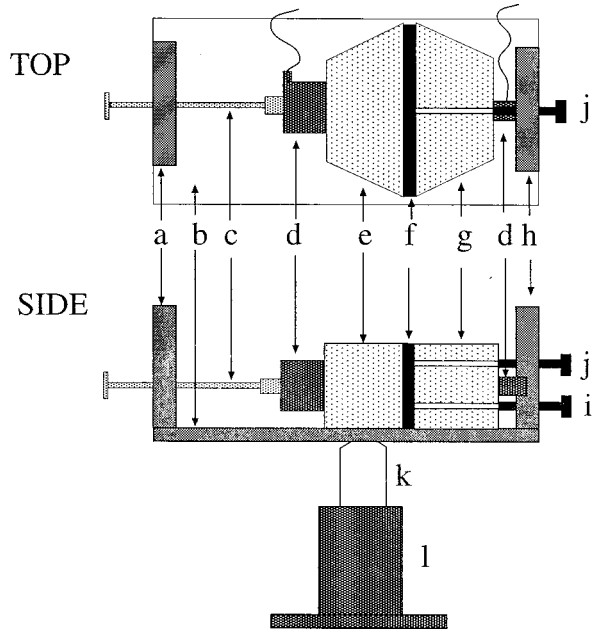

FIG. 1. Layered prism photoacoustic cell: a=stainless steel union with tapped hole for tension device, b=baseplate, c=tension device, d=transducers, e=front prism, f=shim, g=prism with inlet and outlet holes, h=stainless steel union with tapped holes for inlet and outlet fittings, i=inlet (Upchurch fitting), j=outlet (Upchurch fitting), k=post, l=post holder.

II. EXPERIMENT

A. Description of layered prism photoacoustic cell

The layered prism photoacoustic cell is assembled from a pair of dovetail prisms, long sides clamped together and separated by a shim with a hole in the center of it (0.1–1 mm, brass or Kalrez), Fig. 1. The dovetail prisms were fabricated from standard right angle prisms by cutting and polishing the 90° corner down to create a parallel surface to the hypotenuse. The cut sides of the dovetail prisms provide two surfaces, parallel to the cell chamber, to clamp a pair piezoelectric transducers. Inlet and outlet holes (1/16 in.) were drilled through one of the prisms to permit flow of the solution through the sample compartment. A union, fabricated from a stainless steel block (1/8 in. thick, 1/4 in. wide, 1/2 in. tall) tapped with holes (1/4 in.-28) centered over the corresponding inlet and the outlet holes in the prism, was attached perpendicular to a base plate that held the prisms parallel to the laser table. Teflon tubing (1/16 in. o.d.) was attached to the inlet and outlet of the prism using flangeless fittings (Upchurch *P*202 nut and *P*240 ferrule). One transducer was clamped to the cell with a Teflon holder attached to the end of a screw threaded through a second stainless steel block attached to the base plate parallel to the solution inlet/outlet union. A second 0.25 in. transducer can be placed between the back prism and the union with the inlet and outlet fittings. The cell was assembled by placing the two prisms separated by a shim on the base plate. The drilled holes were aligned with the flangeless fittings in the stainless steel block union. The front transducer was brought in contact with the cell by adjusting the tension of the Teflon holder. Silicon vacuum grease was used to provide acoustic coupling between the LPC and the piezoelectric transducers. Simple finger tightening of the low pressure flangeless fittings provides the final clamping adjustments for the cell providing a robust, leak-tight connection. The sample was either pushed through the cell with a syringe pump or pulled through using a peristaltic pump.

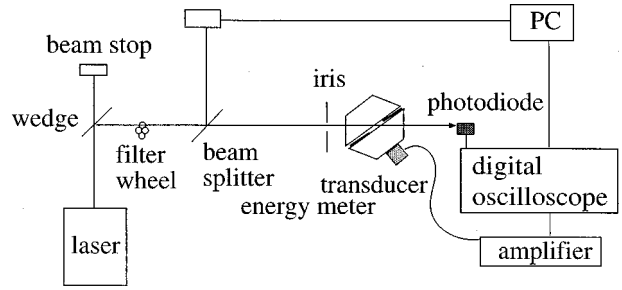

FIG. 2. Schematic of experimental setup.

B. Experimental method

A diagram of the experimental arrangement is shown in Fig. 2. The excitation source [Lambda Physik Excimer XeCl 308 nm; 20 ns full width at half maximum (FWHM) or a Continuum Surelite Nd:yttrium–aluminum–garnet (YAG) 355 nm; 15 ns FWHM] is aligned normal to the air/prism interface. Using a cell made from a pair of prisms allows the light to be transmitted through the sample and provides two surfaces parallel to the propagating planar acoustic wave to couple a pair of piezoelectric transducers. Total internal reflection of the light incident on a right angle 45° prism occurs at a quartz air interface at angles less than the critical angle ($\theta_c \sim 42.5°$).[35] However, the light can be efficiently refracted if the air interface is replaced by a higher refractive index medium (for water or acetonitrile $\theta_c \sim 64°$). Therefore, if the laser beam is aligned normal to the air/quartz prism interface, the light passes through the cell and arrives at a 45° angle incident to the quartz/liquid interface. At this acute angle, the light from the pulsed laser is refracted through the sample and out the opposite prism generating an acoustic wave that propagates through the dovetail prism *normal* to the clamped transducer as illustrated in Fig. 3. Alternatively, a modified hemispherical prism could be used to couple light

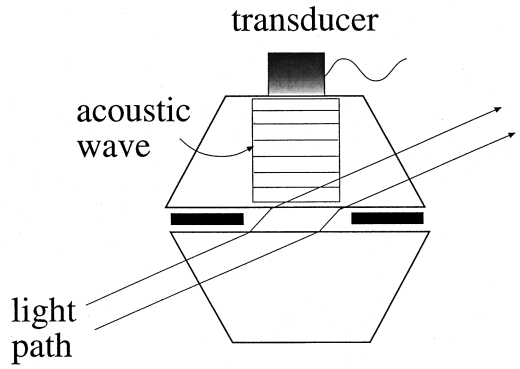

FIG. 3. Light transmitted through the layered prism cell generates an acoustic wave parallel to the transducer. The planar acoustic pressure wave propagates through the prism at the speed of sound.

Downloaded 06 May 2003 to 198.128.86.151. Redistribution subject to AIP license or copyright, see http://ojps.aip.org/rsio/rsicr.jsp

into the liquid sample chamber, so long as the top of the prism is ground down parallel to the sample chamber to provide a surface for the transducer.

The signals from the transducers were amplified (either a Panametrics 5670 w/50 Ω input impedance or a SRS240 DC-300 MHz). In a typical photoacoustic experiment, the averaged photoacoustic waveforms (1 and 5 MHz) from the sample, the solvent, and a reference were collected on a two-channel digital oscilloscope (Lecroy 7200, operating at 1 ns per point) and transferred to a computer for data analysis. Part of the laser beam was monitored with an energy meter before the photoacoustic cell to normalize the acoustic waveforms (reference, sample, background) for any drift in the laser power over the time of the experiment.

In our later work we used a photoacoustic spectrometer developed for use in PNNLs Environmental Molecular Sciences Laboratory. Sound Acquisition V1.26E [Quantum Northwest (QNW), Spokane, Washington] greatly simplified data acquisition and data transfer and provided computer control of the experimental hardware; peristalic pump (Masterflex, model 7521-50) to flow samples; a six-port selection valve (Upchurch V341 valve and V1000 actuator) to change from sample, reference, and background solutions, a TASC 300 (QNW) cell holder (modified to hold the LPC) to provide temperature control, and a shutter (Uniblitz D122 controller and VS25S1S0 shutter) to block the laser during temperature stabilization. Variations in the laser power were monitored with a pyroelectric energy probe (QNW EPPYR). The PA waveforms were collected on a digital oscilloscope (Lecroy 7200) and transferred over (GPIB) to a computer for data analysis.

1. Materials

All chemicals and solvents used in this work were purchased from Aldrich, except potassium chromate purchased from Baker (analyzed reagent grade). The organic solvents were HPLC grade and used without further purification. Benzophenone (Bp) and *o*-hydroxy-benzophenone (OHB) were purified by recrystallization in methanol. A Perkin Elmer 552A UV-Vis Spectrophotometer was used to measure absorbances of the reference and sample solutions.

In our experiments either a 0.25 in. Panametrics 5 MHz (model A110S) transducer, a 0.5 in. Panametrics 1 MHz (V103), a 0.5 in. Stavley 1 MHz (model K-M) transducer, or an air-backed 0.25 in. PZT-5A piezoelectric crystal (Valpey–Fisher) was used. The 5 MHz is more sensitive for the faster events (<20 ns) and the 1 MHz is more sensitive for the slower events (>200 ns).

2. Deconvolution methods

Time-resolved analysis was accomplished by convolution methods in the time domain with either the software package SoundAnalysis3000[36,37] (V1.13) from Quantum Northwest (Spokane, Washington) or with the program C2NLIN[20] shared by the UT Dallas group. One full cycle of the acoustic waveform was used in the data analysis including at least 25 channels prior to the rise of the signal to provide a baseline. Using a pair of transducers permits analysis of a greater time range and provides an additional confirmation of the results obtain from the convolution analysis.

3. Benzophenone triplet quenching by potassium iodide

Solutions containing benzophenone and potassium iodide (Bp/KI) were prepared in 90/10 v/v acetonitrile/water mixture (absorbance $0.71-0.75\ \mathrm{cm}^{-1}$ at 355 nm). For each Bp/KI solution, a reference solution (OHB/KI) was prepared by matching absorbance ($\pm 2\%$) with the corresponding (Bp/KI) sample. The solutions were purged at room temperature with nitrogen just prior to analysis.[38] In the photoacoustic experiment, the sample, reference, and solvent (background) were flowed through the prism cell (0.5 mm Kalrez shim) using a peristaltic pump (3.1 mL/min). The attenuated output of the Nd:YAG laser (355 nm, 10 Hz) was passed through a 5 mm iris to provide 190 μJ/pulse entering the LPC. The photoacoustic waveforms obtained from averaging 100 lasers shots were normalized to the average laser power measured with a power meter and stored on a computer for data analysis. The experiment was repeated in triplicate at each KI concentration.

4. Hydrogen transfer kinetics

Solutions of ethanol/methanol mixtures (100/0, 75/25, 50/50, 25/75, 0/100 v/v) were prepared and added to volumetric flasks containing 6% volume of *tert*-butyl peroxide after final dilution. Reference solutions of OHB in ethanol/methanol mixtures were prepared by matching the absorbances to the samples containing the *tert*-butyl peroxide in 1 cm cuvettes ($\pm 2\%$, absorbance $0.4\ \mathrm{cm}^{-1}$ at 308 nm). In the photoacoustic experiment, the sample, reference, and solvent (background) were flowed through the prism cell (0.5 mm shim) using a peristaltic pump. The attenuated output of the XeCl laser (308 nm, 275 μJ, 5 Hz) is passed through a 5 mm iris before entering the LPC. The photoacoustic waveforms obtained from averaging 100 lasers shots were normalized to the average laser power measured with a power meter and stored on a computer for data analysis. Each experiment was repeated three times.

III. RESULTS AND DISCUSSION

A. Phenomenalogical description of photoinduced acoustic waves

In a pulsed photoacoustic experiment, absorption of light by a solute in a solvent generates an electronically and/or vibrationally excited metastable intermediate. An acoustic pressure wave is generated by a volume expansion due to the local increase in temperature from the nonradiative decay process:

$$\begin{aligned} &M + h\nu \rightarrow M^*, \\ &M^* \rightarrow M + \text{heat}. \end{aligned} \tag{I}$$

The pressure waves generated by heat released from nonradiative decay (i.e., internal conversion and/or vibrational relaxation) of the solute M^* and by electrostriction of the sol-

Downloaded 06 May 2003 to 198.128.86.151. Redistribution subject to AIP license or copyright, see http://ojps.aip.org/rsio/rsicr.jsp

vent can be detected with an ultrasonic transducer. The wave equation[39] governs the relationship between the photoinduced acoustic pressure wave (p) and the time profile of the intensity of the laser pulse (I) as shown in

$$(1/v_s^2\partial^2/\partial t^2-\nabla^2)p=(K_a\partial/\partial t-K_e\partial^2/\partial t^2)I, \tag{1}$$

where v_s is the velocity of sound, K_a is an absorption term and K_e is an electrostriction term. For optically dilute solutions and nanosecond pulsed lasers it can be seen from Eq. (1) that the two components contributing to the observed photoacoustic signal, absorption, and electrostriction, will differ in shape and amplitude. The contribution due to absorption is proportional to the first derivative of the intensity of the excitation source in time and a solvent-dependent term K_a. The solvent-dependent parameters defining the magnitude of the absorption term are the absorption coefficient (A), the thermal coefficient of expansion (β), and the heat capacity (Cp) of the bulk solvent as shown in

$$K_a=A\beta/Cp. \tag{2}$$

On the other hand, the contribution to the photoacoustic signal due to electrostriction of the solvent is proportional to the second derivative of the intensity of the excitation source in time and an electrostriction term K_e. The electrostrictive parameters shown in

$$K_e=\gamma/2ncv_s^2 \tag{3}$$

are the refractive index of the solvent (n), the speed of light (c), the velocity of sound in the solvent (v_s), and an electrostrictive coefficient (γ), as shown in

$$\gamma=(n^2-1)+1/3(n^2-1)^2. \tag{4}$$

When the absorption coefficient (A) is large, the PA signal is dominated by the absorption term and the electrostriction term may be neglected. However, for optically dilute solutions the electrostrictive term may bound the limit of detection in the PA experiment. The sensitivity of either the LPC or the LRC is characterized by the density of the absorbed energy, i.e., microjoules absorbed by the solute per microliter of excitation volume. On the other hand, we will show the experimental sensitivity for cuvette cell depends not only on the energy density, but also depends significantly on the diameter of the excitation source.

In the following sections, the physical parameters describing (1) the absolute magnitude of the photoinduced acoustic pressure wave in a variety of solvents, (2) the time response of the PA signal as a function of cell geometry, and (3) the limits of detection as confined by the background contributions are presented. An analysis of the fundamental physical parameters describing the pressure change induced by the absorption and electrostriction under optically dilute conditions provides a basis for characterizing the similarities and differences between the three photoacoustic cell geometries. The acoustic pressure wave produced in the LPC and the LRC is described by most of the same unique features. The only significant difference between the two cell geometries is the absence of a rear reflector in the LPC. By eliminating the reflector, we have increased the flexibility of the layered cell geometry in two ways: (1) no background signal due to absorption by the reflector, and (2) the cell can be used at any wavelength in the UV-vis, near-IR range.

B. Photoinduced pressure change, conversion of optical energy to mechanical energy

The magnitude of energy released as heat (ΔT) to the solvent induced by absorption of light can be calculated in

$$\Delta T=[1/(Cp\rho)][(H_{\text{th}}/V_0)] \tag{5}$$

from the thermoelastic properties of the bulk solvent and density of the absorbed energy, where Cp is the molar heat capacity (joules/°C g) V_0 is the excitation volume and ρ is the density (g/mL) of the bulk solvent. The energy absorbed by the sample, H_{th} (joules) is calculated in

$$H_{\text{th}}=E_{h\nu}(1-10^{-A}) \tag{6}$$

from the absorbance of the sample (A) and the energy of the excitation source ($E_{h\nu}$). The increase in pressure due to the local heating of the solvent molecules can be calculated by

$$\Delta P=\Delta T(\beta/\alpha) \tag{7}$$

from the change in temperature (ΔT) and the thermal pressure coefficient of the solvent. where β is the thermal coefficient of expansion (1/°C) and α is the isothermal compressibility (1/Pa). Substitution of the terms that describe the ΔT in Eq. (5) into Eq. (7) provides a calculation of the magnitude of pressure change dependent on experimentally measurable parameters, as shown in

$$\Delta P=[\beta/\alpha Cp\rho][H_{\text{th}}/V_0]. \tag{8}$$

Inspection of Eq. (8) shows that the photoinduced pressure change is equal to the product of a ''solvent quality factor'' [40] $[\beta/\alpha Cp\rho]$ and the density of the absorbed energy $[H_{\text{th}}/V_0]$ in the photoacoustic cell. Using Eq. (8), the absolute magnitude of the pressure change, ΔP, for any photoacoustic experiment can be determined with a knowledge of the solvent quality factor and an experimental measure of the energy density in the photoacoustic experiment. Table I provides a comparison of the calculated pressure change for absorption of light by a photoacoustic standard (excited state lifetime <1 ns, Φ internal conversion equal to 1.0) in a series of solvents assuming an energy density of 1 μJ/μL. Examination of the calculated pressure change in Table I shows that photoinduced pressure change will vary significantly based on the differences between the thermoelastic properties of the solvents.

Although the ΔT for absorption of 1 μJ/μL is quite small, the induced pressure change is of the magnitude easily detected by a piezoelectric transducer.

C. Calculation of photoacoustic signal amplitude, conversion of mechanical to electrical energy

Given the absolute magnitude of the photoinduced pressure wave (ΔP, Table I), the amplitude of the photoacoustic signal obtained from a piezoelectric transducer can be estimated using

$$\text{PA signal (voltage)}=K^*f^*\Delta P, \tag{9}$$

Downloaded 06 May 2003 to 198.128.86.151. Redistribution subject to AIP license or copyright, see http://ojps.aip.org/rsio/rsicr.jsp

TABLE I. Absolute magnitude of the pressure change (ΔP) in Pascals (Pa) as a function of solvent composition. The magnitude of ΔP assumes a density of absorbed energy of 1 μJ/μL.[a]

Solvent	β ($\times 10^{-3}$) (1/°C)	α ($\times 10^{-10}$) (1/Pa)	Cp J/gm °C	ρ gm/mL	ΔT ($\times 10^{-4}$) °C	ΔP Pa
water	0.257	4.58	4.184	1	2.4	135
methanol	1.19	12.2	2.54	0.76	5.0	579
ethanol	1.08	11.1	2.39	0.79	5.3	519
2-propanol	1.04	11.0	2.57	0.79	5.0	471
acetonitrile	1.37	10.7	2.18	0.78	5.9	756
heptane	1.22	14.1	2.25	0.68	6.8	584
benzene	1.22	9.4	1.74	0.87	6.6	848
toluene	1.08	9	1.64	0.87	7.0	843
CCl4	1.27	10.4	0.86	1.58	7.3	894

[a]Thermoelastic constants obtained from Refs. 41–43.

where (K) is a ''transducer constant'' containing the piezoelectric parameters[7,28] for conversion of mechanical to electric energy and (f) is the efficiency of energy transfer (acoustic impedance) from the sample to the transducer. The transducer constant K (units μV/Pa) is calculated from

$$K=(K_{33}d_{33}h)/(\epsilon_0\epsilon_r), \tag{10}$$

where K_{33} is a dimensionless coupling factor, d_{33} is the piezoelectric charge constant (C/N), h is the thickness of transducer (proportional to the frequency constant), ϵ_0 is the dielectric constant (8.85×10^{-12} A S/Vm), and ϵ_r is the relative dielectric constant (dimensionless).

The fraction of energy transferred through an interface can be estimated from the acoustic impedance at the interface of the various layers. The derivation of the fraction of energy transferred through a water/quartz interface where Z_w and Z_q are the acoustic impedance of water and quartz, respectively, is shown as

$$f=1-[(Z_w-Z_q)^2/(Z_w+Z_q)^2]. \tag{11}$$

Table II provides a comparison of the calculated PA signal magnitude (μV/Pa) for a series of piezoelectric transducer elements. Two observations are notable: First, there are only small differences in the calculated magnitude of photoacoustic signals for most of the ceramic transducers. Second, the signal obtained from the thin film polymeric piezoelectric materials, polyvinyldifluoride (PVDF) transducer is estimated to be between 1 and 2 orders of magnitude lower than the signal obtained for a 1 MHz ceramic piezoelectric transducer. Thus, either greater amplification or higher energy densities (>1 μJ/μL) will be required to obtain a comparable signal from the polymeric piezoelectric materials.

Table III provides a comparison of the calculated PA signal amplitude with the PA signal amplitude measured in the LPC using a 5 MHz lead zirconate titanate (PZT-5A) transducer. The agreement between the calculated and the observed signals is quite satisfactory. The greatest uncertainty in the calculated value most likely arises from the estimate of acoustic energy transfer between the quartz/couplant/piezoelectric transducer interfaces.[47]

The data provided in Tables I and II yields a method, *a priori*, to calculate the reaction conditions necessary to observe an acoustic signal from a PA standard in the layered prism cell for a variety of commercially available piezoelectric transducers. For example, a density of absorbed energy equal to 1 μJ/μL will yield a signal of $\sim$0.9 mV in water ($\sim$5 mV in acetonitrile) using a 5 MHz PZT transducer, with no amplification! The data provided in Table III demonstrates empirically that energy densities as low as tenths of microjoules per microliter provide a readily measurable signal with only moderate (20 dB) amplification.

D. Limits of detection and sensitivity of optical dilute solutions

Both the limit of detection (LOD) and the sensitivity of photoacoustic spectroscopy depend on the geometry of the photoacoustic cell. The limit of detection is defined as the minimal detectable absorbance by a solute dissolved in a

TABLE II. Mechanical to electrical conversion constants for piezoelectric transducers coupled to the layered prism cell. The data permit a comparison of the relative magnitude of the signal obtain with a 5 MHz transducer per Pascal of pressure change for a series of piezoelectric materials.

Material	Freq Const[a]	K_{33}	Kp	d_{33}	f (total)	Z_p	ϵ_r	μV/Pa
PZT(5A)	1.88	0.7	0.58	374	0.05	30	1700	6.5
K-83	2.65	0.38	0.1	65	0.07	23	175	8.5
Nova(3B)	2.16	0.5	0.01	70	0.05	33	215	7.9
Quartz	2.87	0.11		2	0.10	13	4.5	3.2
pvdf[b]	1.5	0.2	0.01	33	0.20	2.7	12	0.05

[a]Refs. 17, 44–47.
[b]Polyvinyldifloride, calculated for 40 μm film.

Downloaded 06 May 2003 to 198.128.86.151. Redistribution subject to AIP license or copyright, see http://ojps.aip.org/rsio/rsicr.jsp

TABLE III. Comparison of the calculated photoacoustic signal and the experimentally observed photoacoustic signal for a standard[a] in the layered prism cell for a 5 MHz piezoelectric transducer,[b] given the density of absorbed energy in nanojoules per microliter of excited volume.

Solvent	density nJ/μL	Calc. signal[c] mV	Measured[a] mV	Calculated/exp't
heptane	138	20.1	21.6	0.9
ethanol	166	21.9	17.2	1.2
acetonitrile	161	31.7	32.8	0.9
toluene	161	35.4	26.2	1.3
CCl_4	161	36.0	26.2	1.3

[a]Photoacoustic standard *o*-hydroxybenzophenone.
[b]$f\sim 4\%$ for acoustic energy transfer through solvent/quartz/couplant/transducer interface.
[c]Gain 20 dB, 5 MHz PZT.

solvent. The sensitivity is defined as the experimental measured signal for a given energy density.

In any photothermal method, the LOD is controlled by the amplitude and reproducibility of the background signal.[29] Given the inherent absence of selectivity in photothermal methods (i.e., anything that absorbs light gives a signal), absorbance by the solvent will always set the absolute LOD. However, in the layered photoacoustic cells, either LPC or the LRC, the signal from electrostriction of the solvent can be greater than the signal due to absorption by the solvent for nanosecond laser pulses. Therefore, electrostriction can determine the limit of detection in a photoacoustic experiment when using the layered cell geometry.

1. Electrostriction

Electrostriction occurs when electromagnetic energy is passed through a dielectric medium. The resulting constriction of the media (solvent) into the region of high electric field results in an acoustic signal. Lai and Young[39] derived an analytical solution to calculate a minimal detectable absorbance ($\alpha_{\min}$) by photoacoustic methods based upon an electrostriction background for several different PA experimental parameters. According to their approach, $\alpha_{\min}$ is defined as the absorbance where the amplitude of the PA signal due to electrostriction is equal to the amplitude of the PA signal due to solute absorption. The next equation provides the relationship between the minimal detectable absorbance, $\alpha_{\min}$, for a spatially Gaussian laser beam and the thermal elastic properties of the solvent; the speed of sound (v_s), the heat capacity (Cp), and the thermal coefficient of expansion of the bulk solvent (β), the refractive index of the media (n), the velocity of light (c), and the electrostrictive coefficient (γ) derived from Eq. (4). Examination of

$$\alpha_{\min}=[(\gamma/2ncv_s^2)\times(Cp/\beta)]/[(\tau_p^2+\tau_a^2)^{1/2}] \tag{12}$$

shows that the magnitude of the electrostriction signal is controlled by two important time scales: the pulse width of the excitation source (τp) and the acoustic transient time (τa). The pulse width of the laser, τp, is defined as the FWHM in units of time and the acoustic transient time, τa, is defined as the time it takes the acoustic wave to travel through the diameter of the laser beam in a cuvette cell.

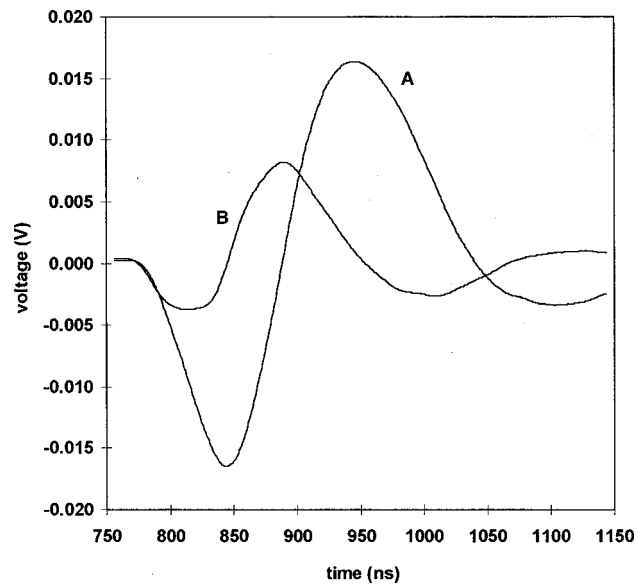

FIG. 4. Comparison of the absorption and electrostriction components of a photoacoustic signal obtained with a 5 MHz transducer coupled to the LPC. A: absorption; OHB in acetonitrile ($A=0.011$/cm) and B: electrostriction; acetonitrile.

One of the unique characteristics of the LPC geometry is the absence of τa in optically dilute solutions due to the homogeneous expansion of the acoustic wave against the cell walls. Because τa is reduced to zero for the layered cell geometry, the contribution of signal due to electrostriction of the solvent is inversely proportional to the pulse width of the laser, τp. Thus, Eq. (12) is reduced to

$$\alpha_{\min}=[(\gamma/2ncv_s^2)\times(Cp/\beta)]/\tau_p \tag{13}$$

for layered photoacoustic cell geometries. Using Eq. (13), $\alpha_{\min}$ is $\sim 1.9\times 10^{-2}$ cm^{-1} in water and 3.1×10^{-3} cm^{-1} in acetonitrile with our Nd:YAG laser (pulse width 15 ns FWHM). For comparison, the absorption coefficient of water[48] at 355 nm is reported to be 4.6×10^{-4} cm^{-1} significantly lower than the LOD set by electrostriction. Therefore, electrostriction, not solvent absorbance, constrains the detection limit for optically dilute solutions and nanosecond laser pulses in any layered cell geometry. Figure 4 compares the PA signal obtained from OHB in acetonitrile in the LPC (absorbance $\sim 1.1\times 10^{-2}$/cm) to the signal obtained from the solvent without solute ''electrostriction background'' (0.5 mm shim, 5 MHz transducer, 355 nm, 800 μJ incident energy, 15 ns FWHM). Three observations are notable: First, the background electrostriction signal is ''out of phase'' with the absorption signal as predicted by the wave equation (the electrostriction component is proportional to the derivative of the absorption component). Second, as predicted from Eq. 13, the signal due to the absorption (33 mV *pk-pk*) is almost three times greater than the signal from electrostriction (12 mV *pk-pk*), for a solute in acetonitrile with an absorption of 1.1×10^{-2} cm^{-1}. Third, with moderate averaging, a PA signal can be obtained with a density of absorbed energy (H_{th}/V_0) down to 50 nJ/μL.[49]

The magnitude of the electrostriction component in the layered cell geometry can restrict its utility in analytical ap-

Downloaded 06 May 2003 to 198.128.86.151. Redistribution subject to AIP license or copyright, see http://ojps.aip.org/rsio/rsicr.jsp

plications requiring very low limits of detection. While the cuvette geometry does not provide the enhanced sensitivity observed with the layered cell geometry, the magnitude of the electrostriction component in the cuvette geometry can be decreased by increasing τa. For example, with a beam diameter of 1 mm, τa is $\sim$900 ns. Even if, τa is 15 ns, using Eq. (12), $\alpha_{\min}$ is $\sim 2.5\times 10^{-5}$ cm^{-1} in acetonitrile compared to $\sim 3.1\times 10^{-3}$ cm^{-1} using the layered cell geometry. Therefore, the cuvette geometry can provide a LOD two orders of magnitude better than either layered cell geometry when using nanosecond pulsed lasers. However, the analytical capabilities of the layered cell geometry can be improved by using a laser with longer pulse widths. For example, a laser with a pulse width of a couple of microseconds would provide the same low LOD in both in a layered photoacoustic cell and cuvette cell geometry.

2. Cell absorbance

Arnaut and co-workers have previously discussed methods to minimize background cell absorbance in the LRC geometry.[21] Replacing the aluminum mirror in the original design with a dielectric reflector significantly reduced the signal due to cell absorbance. The only drawback is that a separate dielectric reflector is required for each laser wavelength (e.g., 266, 308, 355, or 532 nm). In addition a second filter set was necessary for experiments using the third harmonic (355 nm) pump from the Nd:YAG to further attenuate the extraneous 532 and 1064 nm fundamental from passing through the dielectric reflector and generating a pyroelectric signal.

The advantage of the LPC design lies in the absence of the reflector and consequently the flexibility to use the same cell over the entire UV-vis and near-IR wavelength region.

E. Time-resolved photoacoustic spectroscopy

Two different approaches have been used to obtain the kinetic information from photoinduced multistep reaction pathways: (1) deconvolution by convolution in the time domain[37] or in the frequency domain[23] and (2) curve fitting of the PA signal intensity as a function of quencher concentration or laser beam diameter.[19,50] Ultrasonic piezoelectric transducers provide the capability to obtain kinetics on a submicrosecond time scale with either the layered cell or cuvette cell geometry. Pulsed PA calorimetry approaches have been used to measure both lifetimes and energetics of excited state intermediates in the presence and absence of quenching agents.[5,51,52] In

$$\begin{aligned} &A + h\upsilon \rightarrow A^{**} \xrightarrow{\tau 1} A^{*}, \\ &A^{*} + Q \xrightarrow{\tau 2} A + Q, \end{aligned} \tag{II}$$

quenching of an excited state intermediate (A^*) by quencher (Q) is described by two sequential reaction steps. In the first step, the transient intermediate A^* is formed by photoexcitation of the ground state molecule A. The rate of formation of $A^*(1/\tau 1)$ is dependent on internal conversion of the excited state A^{**}, and the fraction of the absorbed photon energy released as heat ($\phi 1$) is proportional to

$$\phi 1 = [E_{h\upsilon}(1-\Phi) + \Phi(E_{h\upsilon} - E^*)]/E_{h\upsilon} \tag{14}$$

where Φ is the quantum yield for formation of A^*, $E_{h\upsilon}$ is the energy of the excitation source, and E^* is the energy of the excited state intermediate A^*. In the subsequent step, the rate of formation of $A(1/\tau 2)$ is dependent on the rate of energy transfer, k_q, and the quencher concentration $[Q]$. The fraction of energy released as heat is proportional to

$$\phi_2 = \Phi(\Delta H_{\text{rxn}})/E_{h\upsilon}, \tag{15}$$

where ΔH_{rxn} is the heat released in forming ground state A from A^*.

Small and co-workers[37] have shown that the PA signal $[S(t)]$ obtained from a resonant transducer can be described by a convolution (denoted by $*$) of the time-dependent relaxation function of the transient intermediate $i[q_i(t)]$, with the instrument response function $[M(t)]$ as shown in

$$S(t) = k\sum \phi_i[M(t)_* q_i(t)], \tag{16}$$

where k is an instrument constant proportional to the optoacoustic pressure change and ϕ_i is the fraction of energy released as heat from intermediate i. The instrument response, $M(t)$, is dependent on both the resonant frequency characteristics of the ultrasonic transducer (υ_t) and the geometry of the experiment (layered or cuvette). When the relaxation function of the transient intermediate $q(t)$ can be described by a first-order or pseudo first-order decay, the function $q_i(t)$ can be modeled as an exponential decay as shown in

$$q_i(t) = (1/\tau_i)\exp(-t/\tau_i), \tag{17}$$

where τ_i is the lifetime of the intermediate. The instrument response for a particular photoacoustic experimental geometry (cuvette or layered cell) is obtain by using a reference compound that has a quantum yield of unity for internal conversion and an excited state lifetime, $\tau \ll 1/\upsilon_t$ where υ_t is the resonant frequency of the transducer. Under these conditions the photoacoustic signal $S(t)$ provides the instrument response. On the other hand when τ is comparable in magnitude to $1/\upsilon_t$, the photoacoustic signal is broadened in frequency and decreased in amplitude due to the successively delayed ''slices'' of the acoustic pressure wave arriving at the detector at times out of phase with the resonant frequency of the transducer.[18] Figure 5 provides a comparison of the instrument response of a 5 MHz transducer ($\tau = 0$, $\phi = 1$, obtained from an OHB/methanol solution) to the heat released from a simulated transient intermediate with a finite lifetime ($\tau = 10$ ns, $\phi = 1$ and $\tau = 100$ ns, $\phi = 1$). If the fraction of photon energy released as heat is less than 1, then the amplitude of the acoustic wave is simply reduced proportionally in amplitude by the fraction, ϕ, released as heat. For example, the amplitude of the acoustic wave generated by a transient intermediate ($\tau = 10$ ns, $\phi = 0.5$) is half the amplitude of the signal when $\phi = 1$. This is an important point—(1) the amplitude of the signal is directly proportional to the amount of heat released, thermodynamics and (2) the shape of the signal is directly proportional to the lifetime of the

Downloaded 06 May 2003 to 198.128.86.151. Redistribution subject to AIP license or copyright, see http://ojps.aip.org/rsio/rsicr.jsp

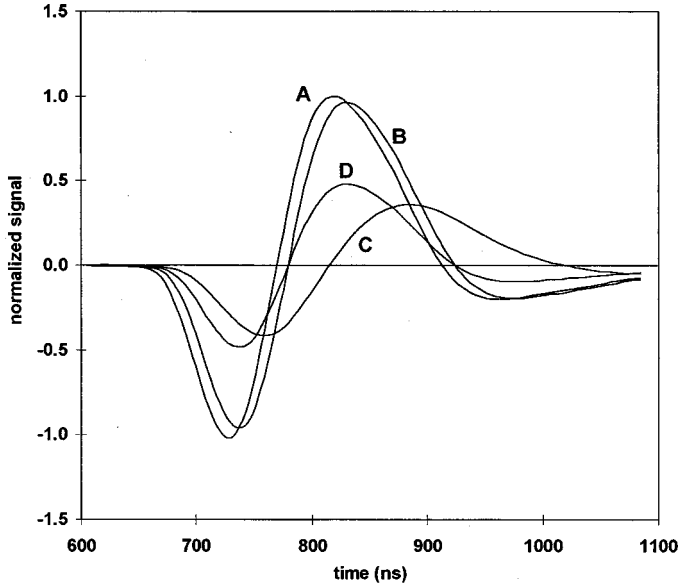

FIG. 5. Photoacoustic response, $S(t)$, obtained by convolution of the relaxation function of a transient intermediate, $q(t)$, with the instrument response $M(t)$. A: $M(t)$; $\tau=0$ ns and $\phi=1$, B: $S(t)$ $\tau=10$ ns and $\phi=1$, C: $S(t)$; $\tau=100$ ns and $\phi=1$, and D: $S(t)$; $\tau=10$ ns and $\phi=0.5$.

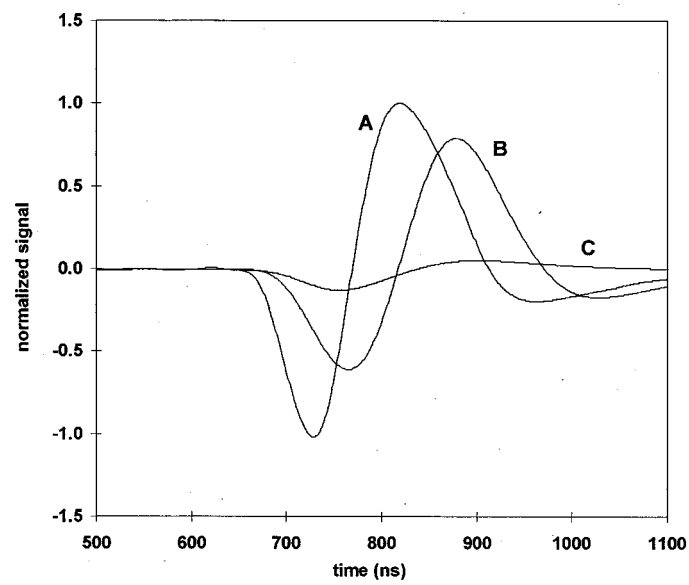

FIG. 6. Comparison of the instrument response function, $M(t)$, for a LPC and a cuvette cell using a 5 MHz transducer. A: LPC, $\tau_a=0$, B: cuvette cell, $\tau_a=100$ ns, C: cuvette cell, $\tau_a=500$ ns.

metastable intermediate (kinetics). Therefore, kinetic information can be obtained independent of the thermodynamic quantities within a given photoacoustic experiment.

1. Comparison of the layered and cuvette cells

The instrument response, $M(t)$, as shown in

$$M(t)=F(t)_{*}I(t) \tag{18}$$

for a given photoacoustic cell geometry is a convolution of the frequency response of the transducer, $F(t)$, and the temporal profile, $I(t)$, of the laser beam, specifically the beam profile as dependent on τa and τp. Consequently, the temporal profile depends on the geometry of the photoacoustic cell; the cuvette geometry is defined by a wide beam $[\tau a > \tau p,\ I(t)\propto \tau a]$, and the layered cell is defined by a narrow beam $[\tau a\rightarrow 0,\ I(t)\propto \tau p]$. This difference is the origin of both the enhanced sensitivity and time resolution of the layered cell geometry compared to the cuvette geometry. In the cuvette cell wide-beam geometry, the experimentally observed photoacoustic signal is broadened because the acoustic wave generated at the top of the excitation volume arrives at a delayed time from the wave generated at the bottom of the excitation volume by $\tau a=v_s/d$, where v_s is the velocity of sound in the solvent and d is the beam diameter. In analogy to the exponential time-dependent release of heat from an excited state intermediate, the successively delayed slices of the acoustic pressure wave from the excitation volume arrive at the detector at times out of phase with the resonant frequency of the transducer. The instrument response in a cuvette cell is the convolution of the frequency response of the piezoelectric transducer with a ''square wave'' with a width equal to the acoustic transient time. Figure 6 compares the instrument response $M(t)$ for the layered cell geometry $(\tau a\rightarrow 0)$ to the cuvette cell geometry for τa of 100 and 500 ns (beam diameter $\sim$110 and 550 μm, respectively). The ''broadening'' of the acoustic waveform by τa is the basis for the lack of sensitivity in the cuvette geometry relative to the layered cell geometry for an experiment with the same absorbed energy density.

2. Acoustic travel time

An additional time frame that hinders kinetic analysis in the cuvette geometry is the acoustic arrival time, τd, defined as the time it takes for the acoustic pulse to arrive at the detector as shown in

$$\tau d=r/va, \tag{19}$$

where r is the distance between the excitation source and the detector and va is the velocity of sound in the media. In the cuvette geometry, τd depends on the velocity of sound v_s in the solvent, whereas in the layered cell geometry, τd is independent of the solvent composition and depends only on the thickness of the cell wall. Because the speed of sound is proportional to the thermoelastic properties of the solvent, any difference between the components of the sample and reference solutions could introduce an artifact in the observed PA signal. Therefore, it is imperative to use the layered cell for kinetic analysis in mixed solvents because the arrival time of the acoustic pulse depends only on the time-dependent relaxation function of the transient intermediate.

Taking advantage of the ability to use the cuvette and LPC at any wavelength in the UV-vis range, an experiment was performed to measure the relative differences between the thermal elastic properties of methanol in the presence and absence of di-*t*-butyl peroxide. The peroxide has little absorbance at 532 nm, and therefore is considered only a solvent component. Iodine was used as a photoacoustic standard since it has a reasonable absorbance at 532 nm to measure the difference in acoustic arrival times, $\Delta\tau d$, in the cuvette

Downloaded 06 May 2003 to 198.128.86.151. Redistribution subject to AIP license or copyright, see http://ojps.aip.org/rsio/rsicr.jsp

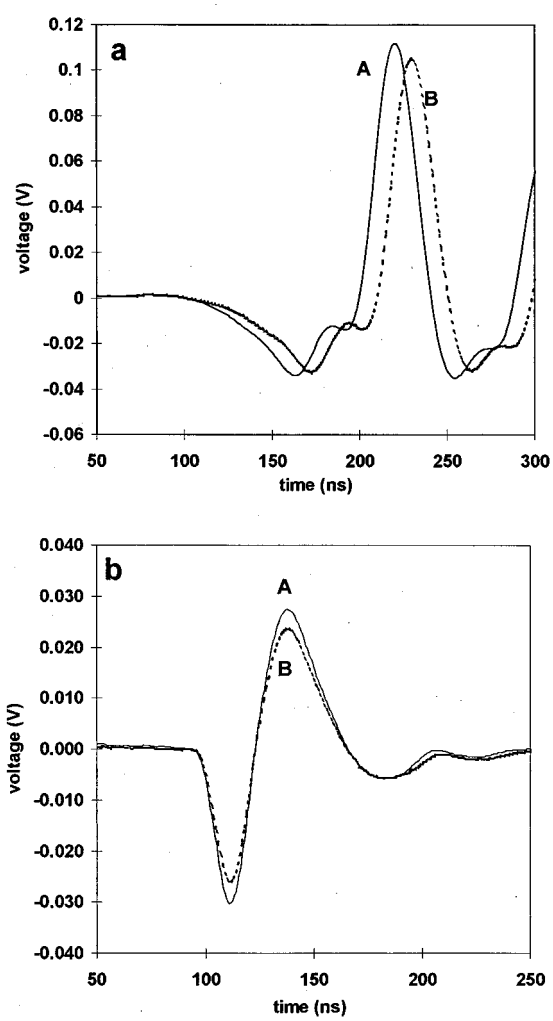

FIG. 7. Comparison of the acoustic arrival time, τ_d, in the (a) cuvette cell and the (b) LPC. A: I_2(A=0.3/cm) in neat ethanol, B: I_2(A=0.3/cm) in 15%(v/v) di-*t*-butyl peroxide/ethanol.

cell. Figure 7(a), shows that addition of peroxide to a solution of alcohol leads to an observed decrease in the velocity of sound, significantly changing the acoustic arrival time in the cuvette cell. Figure 7(b) shows that the arrival time, τd, of the acoustic wave in the LPC is independent of the thermoelastic properties of the solvent thus demonstrating the ability of the LPC to measure kinetics in mixed solvents. However, it should be noted that in Fig. 7(b), the magnitude of the acoustic wave decreases with increasing peroxide concentration because the amplitude of the acoustic wave is not independent of the bulk solvent properties. This fact requires caution in attempting to obtain thermodynamic data for the hydrogen abstraction pathway because the thermochemistry is dependent on the amplitude of the signal.

F. Kinetic applications

Kinetic studies of complex reaction mixtures on the nanosecond time scale with the layered prism cell are possible because: (1) the arrival time of the acoustic signal is independent of the bulk properties of the solvent and (2) the response of the piezoelectric transducer is not broadened by the acoustic transient time. In the following section, the enhanced time resolution of the layered prism cell is demonstrated using a well-characterized photochemical standard; benzophenone triplet quenching by potassium iodide. In addition, the lifetime of the reactive *tert*-butoxyl radical in a mixture of organic solvents is measured using the LPC. The photoacoustic results obtained in the layered prism cell are compared to those previously reported using indirect transient absorption techniques.

1. Benzophenone triplet quenching by potassium iodide

Benzophenone (Bp) triplet quenching by potassium iodide (KI) has previously been used as a standard to demonstrate the time-resolved/calorimetry capabilities of pulsed PA spectroscopy. Photolysis of Bp results in efficient triplet formation within a few picoseconds ($\tau 1 \ll 0.1$ ns, $\Phi = 1$). The triplet excited state of benzophenone (Bp*3) has a lifetime ($\tau 2$) of microseconds in the absence of a quencher, however in the presence of KI, the lifetime is decreased by an electron transfer mechanism regenerating the ground state Bp and heat[53] as shown in.

$$\begin{aligned} &\mathrm{Bp} + h\nu \rightarrow \mathrm{Bp}^*1 \rightarrow \mathrm{Bp}^{*3}, \\ &\mathrm{Bp}^{*3} + \mathrm{KI} \rightarrow \mathrm{Bp} + \Delta. \end{aligned} \tag{III}$$

The fraction of energy released as heat in the first step ($\phi 1$) is proportional to the triplet energy of Bp as shown in

$$\phi 1 = [E_{h\nu}(1-\Phi) + \Phi(E_{h\nu} - \mathrm{Bp}^*)]/E_{h\nu}. \tag{20}$$

The fraction of energy released as heat ($\phi 2$) in the quenching step is proportional to the ΔH_{rxn} of the quenching event, where Φ is the quantum yield of triplet formation ($\Phi = 1$) and $E_{h\nu}$ is the energy of the excitation pulse (355 nm, 80.1 kcal/mol), as shown in

$$\phi 2 = \Phi(\Delta H_{\mathrm{rxn}})/E_{h\nu}. \tag{21}$$

The lifetime of Bp* ($\tau 2 = 1/k_q$) is proportional to the sum of its unimolecular decay ($\tau 2'$) the concentration of [KI], and the rate of energy or electron transfer (k_q) as shown in

$$\tau 2 = \tau 2' + 1/kq[\mathrm{KI}]. \tag{22}$$

The slope of a plot of $1/\tau 2$ observed versus the quencher concentration provides the rate constant for quenching. In early work, Heihoff and Braslavsky measured a k_q of 7.8×10^9 $\mathrm{M}^{-1}\,\mathrm{s}^{-1}$ in a 4/1 v/v acetonitrile/water solution using a cuvette photoacoustic cell.[50] However, their time resolution was limited to lifetimes $\tau 2 > 60$ ns due to broadening of the signal by the acoustic transient time. Attempts to decrease the acoustic transient time by focusing the laser to a smaller diameter can lead to artifacts due to photon saturation. A laser beam diameter between 1 and 2 mm is generally recommended to avoid artifacts due to absorption of two sequential photons in the cuvette geometry,[37] consequently this will yields τa's ~ 1 to 2 μs.

Recently, Ni and Melton[33] using their ''front-face'' layered cell design demonstrated the enhanced time-resolution capabilities of the LRC. They measured a k_q of 4×10^9 $\mathrm{M}^{-1}\,\mathrm{s}^{-1}$ in a 9/1 v/v acetonitrile/water solution and demonstrated the ability to measure lifetimes down to 3 ns.

Downloaded 06 May 2003 to 198.128.86.151. Redistribution subject to AIP license or copyright, see http://ojps.aip.org/rsio/rsicr.jsp

TABLE IV. Stern–Volmer analysis ($1/\tau 2$ vs [KI]) for benzophenone triplet quenching in a layered prism cell for a 1 and 5 MHz transducer. Weighted least squares analysis of 5 MHz data yields k_q of 4.3 $\times 10^9$ M^{-1} s^{-1}.

1MHz [KI] mM	$\tau 2$ (ns)	%RSD[a]	Et (kcal/mol)	$(\phi 1+\phi 2)$	5 MHz $\tau 2$ (ns)	%RSD[a]	Et (kcal/mol)	$(\phi 1+\phi 2)$
0.5	421	4.3	68.2	1.01	442	5.3	68.3	1.08
1	220	2.2	65.5	1.13	225	6.4	66.9	1.12
2.5	108	2.3	66.9	0.96	105	4.5	69.1	0.96
5	47	1	66.9	1.0	46	1.9	68.7	0.98
10	22	2.3	68.7[b]	1.0	23	1.7	68.7[b]	1.0
25	6.3	3.5	68.7[b]	1.08	8.1	4.8	68.7[b]	1.05
50	3.2	6.1	68.7[b]	1.01	4.9	15.1	68.7[b]	1.01
100	1.7	17	68.7[b]	0.99	3.3	23.9	68.7[b]	0.98
175	.69	55.3	68.7[b]	0.97	1.8	29.7	68.7[b]	0.98
250	.24	42.5	68.7[b]	0.99	2.0	59.1	68.7[b]	1.00

[a]%RSD error from 2–5 independent PA experiments.
[b]Triplet energy fixed at 68.7 kcal/mol.

A polyvinyl difloride (pvdf) transducer was coupled to their LRC allowing broadband detectability, however relatively high concentrations of Bp (55 mM) were used due to the meager sensitivity of the polymeric detector.

In this work, PA waveforms were collected with both 1 and 5 MHz transducers acoustically coupled to opposite sides of the LPC. The enhanced flexibility of the prism cell is evident from the ability to perform the experiment with either the XeCl excimer (308 nm) or the third harmonic of the Nd:YAG (355 nm) as the excitation source and the ability to collect data with two transducers simultaneously. The data shown in Table IV were taken for a 7.5 mM solution of Bp in a 9/1 v/v solution of acetonitrile/water with varying concentrations of KI (0.5 mm shim, absorbance of Bp at 355 nm $\sim$0.036/cell). Figure 8 shows the observed 5 MHz response from photoexcitation of OHB, and Bp at 5 and 50 mM KI. The heat evolved from the exothermic energy transfer results in experimentally observed broadening of the sample acoustic wave compared to the fast heat evolved from a PA standard. Deconvolution of the photoacoustic waveforms after subtraction of the solvent background provides the lifetime of Bp^{*3} as a function of [KI]. A weighted linear regression of the observed rate of quenching $(1/\tau 2)$ versus quencher concentration for the 5 MHz data is shown in Fig. 9. The slope of a weighted least squares fit of the data provides a k_q (4.3×10^9 M^{-1} s^{-1}). The fastest time resolution we were able to obtain with the 5 MHz transducer was 5 ns. It is apparent from the data shown in Table IV, that the 1 MHz transducer does not provide accurate lifetimes below 20 ns. A weighted linear regression of the 1 MHz data, at concentrations between 0.5 and 25 mM KI, yields a k_q (4.4 $\times 10^9$ M^{-1} s^{-1}).

2. Kinetics measurements in mixed solvents. Hydrogen abstraction by tert-butoxyl radical from ethyl and methyl alcohol

One crucial requirement necessary to obtain either kinetic or calorimetric information using the cuvette photoacoustic cell is to match the ''bulk solvent properties'' of both the sample and reference solutions. Unfortunately this re-

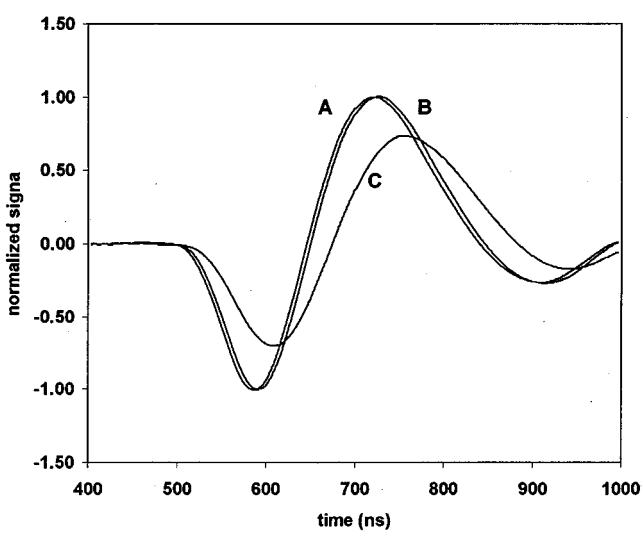

FIG. 8. Comparison of the photoacoustic signal of $S(t)$ obtained from Bp quenching by KI to the instrument response $M(t)$ obtained from OHB. A: OHB, B: Bp, 50 mM KI, C: Bp, 5 mM KI.

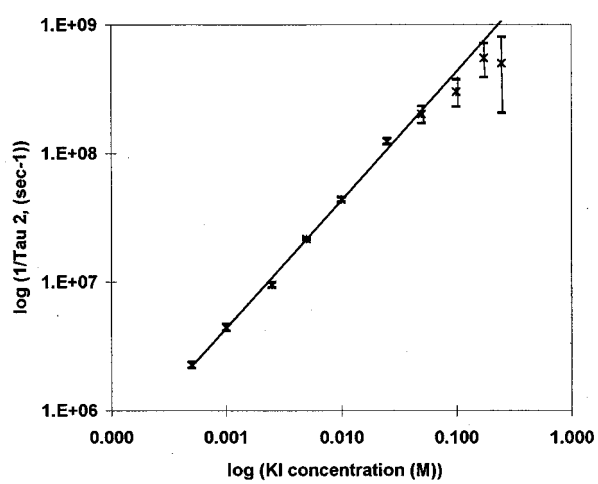

FIG. 9. log/log plot of $1/\tau_{obs}$ vs [KI]. Weighted linear regression yields the quenching rate constant for Bp^{*3} quenching by KI in 9/1 v/v acetonitrile/water; $k_q=4.3\times 10^9$ M^{-1} s^{-1}.

Downloaded 06 May 2003 to 198.128.86.151. Redistribution subject to AIP license or copyright, see http://ojps.aip.org/rsio/rsicr.jsp

quirement restricts the utility of the cuvette geometry to the study of transients derived from photoprecursors at sufficiently low concentrations as not to significantly perturb the bulk solvent properties. On the other hand, one of the inherent beneficial characteristics of the layered photoacoustic cell is the uniform and homogeneous expansion of the sample volume. The acoustic arrival time is independent of the bulk solvent properties, therefore, the time-dependent release of heat can be reconstructed from the ''shift in phase'' of the sample waveform from the reference waveform in mixed solvents.

As a result of the homogeneous expansion in the LPC, a direct measure of the rates of hydrogen abstraction by the alkoxy radical, *tert*-butoxyl radical, from a series of hydrogen donor solvents is possible, even when concentrations of the radical precursor, di-*tert*-butyl peroxide are as high as 10%–20%. However, caution must still be used in attempts to abstract calorimetric information from the amplitudes of the photoacoustic waveforms.[14]

As shown in,

$$t\text{-BuOOBu-}t + h\nu \rightarrow 2t\text{-BuO}(.),$$
$$t\text{-BuO}(.) + \text{SH} \xrightarrow{k_{\text{abs}}} t\text{-BuOH} + S(.) + \text{heat}. \tag{IV}$$

Photolysis of di-*tert*-butyl peroxide at 308 nm yields a pair of *tert*-butoxyl radicals. In the presence of hydrogen donor solvents the *tert*-butoxyl radical abstracts a hydrogen from the solvent to form *t*-BuOH and the solvent radical, scheme IV. The lifetime of the *tert*-butoxyl radical varies from a few nanoseconds to a few microseconds, dependent on the hydrogen donating ability of the donor solvent.

The heat evolved from the exothermic hydrogen atom transfer results in experimentally observed broadening of the sample acoustic wave compared to the fast heat evolved from a PA standard. Deconvolution of the acoustic waveform yields the lifetime of *tert*-butoxyl radical from which the rate of hydrogen abstraction from ethanol (k_{EtOH}) can be derived as shown in

$$1/\tau 2 = k_{\text{EtOH}}[\text{EtOH}]. \tag{23}$$

Using our measured rates of hydrogen abstraction in neat methanol and ethanol, the lifetime of the *tert*-butoxyl radical in a mixture of the two solvents can be calculated assuming one solvent does not affect hydrogen abstraction in the other. In this experiment, the hydrogen being transferred to the alkoxyl radical is from either the C–H α or β to the hydroxyl group so we assume little interaction from hydrogen bonding of the hydrogen atom being transferred to the alkoxyl radical. Table V summarizes the photoacoustic measured lifetime of the *tert*-butoxyl radical in the mixed solvents and the calculated lifetime of the *tert*-butoxyl radical from the composite rate of hydrogen abstraction by the mixed solvent according to

$$1/\tau_{\text{obs}} = k_{\text{obs}} = k_{\text{MeOH}}[\text{MeOH}] + k_{\text{EtOH}}[\text{EtOH}]. \tag{24}$$

The linear correlation, Fig. 10, suggests that hydrogen abstraction in methanol is not affected by the presence of ethanol and vice versa within the experimental error.

TABLE V. Experimentally observed and calculated lifetimes of *t*-butoxy radical, generated by 308 nm photolysis of di-*t*-butylperoxide (6% by volume), in mixtures of methyl and ethyl alcohol.

Solvent [M][a]		tau (ns)		k_{abs} ($\text{M}^{-1}\,\text{s}^{-1}$)
[MeOH]	[EtOH]	observed	calculated[b]	
0	16.1	66± 8[c]	⋯	$9.5\pm1.1\times10^5$ (11×10^5)[d]
5.8	12.1	85±8	79±9	
11.6	8.1	106± 20	98± 10	
17.4	4.0	135± 18	131± 14	
23.2	0	198± 15	⋯	$2.2\pm4\times10^5$ (2.9×10^5)[d]

[a]Solvent concentration corrected for 6% volume of di-*t*-butyl peroxide.
[b]Calculated $1/\tau_{\text{calc}} = k_a^{\text{MeOH}}[\text{MeOH}] + k_a^{\text{EtOH}}[\text{EtOH}]$.
[c]Error in lifetime reported at 95% confidence level.
[d]Literature value from reference.

The lifetimes of the *tert*-butoxyl radical measured in neat ethanol and neat methanol are longer than the lifetimes previously reported by an indirect transient absorption method.[54] The correlation between the calculated and measured lifetimes as a function of solvent composition as shown in Fig. 10 provides additional confidence in our experimental precision. Combined with the recent report[8] that the rate of hydrogen abstraction by *tert*-butoxyl radical from tetrahydrofuran (THF) is nearly a factor of 2 slower than measured in the transient absorption work suggests that the *tert*-butoxyl radical may not be as reactive as previously believed. Further work is in progress to examine the lifetime of the *tert*-butoxyl radical in a series of other organic solvents.

IV. DISCUSSION

In the proceeding sections we have described a new layered photoacoustic cell that uses a pair of prisms to couple the light into and away from the fluid sample. This layered prism cell (LPC) enhances the flexibility of the PA spectroscopist. Specifically, the LPC combines the enhanced time resolution inherent to the front-face irradiation scheme with the zero background inherent to the cuvette geometry. We have shown that LPC can be used to measure transient life-

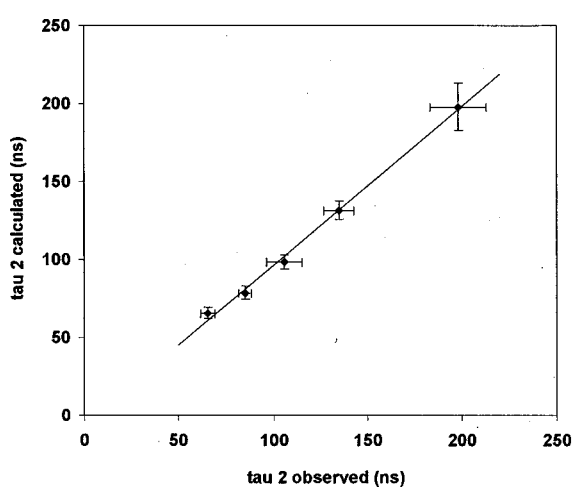

FIG. 10. Comparison of the calculated and observed lifetime of *tert*-butoxyl radical.

Downloaded 06 May 2003 to 198.128.86.151. Redistribution subject to AIP license or copyright, see http://ojps.aip.org/rsio/rsicr.jsp

times down to a few nanoseconds with as little as a 100 nJ absorbed energy per pulse with moderate signal averaging. To demonstrate the unique capability of the layered cell geometry we measure the rates of hydrogen abstraction by *tert*-butoxyl radical from donor solvents by photoacoustic methods in the presence of mixed solvents.

Comparison of LPC to previous cell designs: Two crucial parameters characterize the sensitivity and time resolution of the layered and cuvette PA cell geometries: (1) the density of the absorbed energy (H_{th}/V_0) and (2) the acoustic transient time, τa. To a first approximation, the PA signal amplitude in the layered cell geometry is dependent on the density of absorbed energy in the analyzed sample[22] while the PA signal amplitude in the cuvette cell is a combination of the density of absorbed energy and the acoustic transient time, τa. We showed for the LPC, that the amplitude of the PA signal could be predicted from a measure of the energy density and a knowledge of the thermoelastic properties of the solvent and piezoelectric constants of the transducer.

One of the goals of this work was to develop a spectroscopic method to measure the kinetics of metastable intermediates with little or no monitorable optical absorbance in mixed solvents. Two special requirements must be met to accomplish this task: (1) avoid artifacts to the time-dependent heat release reflected in the experimentally observed phase shift due to changing the thermoelastic properties of the solvent in the reference and in the sample, and (2) the ability to obtain nanosecond time resolution with optically dilute samples.

The LPC offers the flexibility necessary to use photoacoustic calorimetry approaches to realize these challenging goals. First, the geometry of the LPC provides thin beam experiments ($\tau a \rightarrow 0$) and the acoustic arrival time, τs, is independent of solvent composition. Second, the sensitivity of the prism cell permits us to measure sample absorbances <0.02 absorbance units/cell because the background signal due to cell absorbance is essentially zero.

While the thin-beam ($\tau a \rightarrow 0$) nature of the LPC results in both an increase in photoacoustic signal sensitivity and enhanced time resolution, this occurs at the expense of increasing the background signal from electrostriction. Using picosecond lasers and higher frequency transducers in order to improve the time resolution into the subnanosecond range with a layered cell will introduce significantly more background because the electrostriction component is inversely proportional to the pulse width of the laser.

While the LPC does increase the flexibility of the photoacoustic spectroscopist, there are still limitations that will need to be addressed with further research. There is still no satisfactory PA approach to measure the thermodynamics (in contrast to the kinetics) of reactive intermediates in samples with varying solvent composition.

ACKNOWLEDGMENTS

This work was funded by the U.S. Department of Energy, Office of Basic Energy Research, Chemical Sciences Division, Process and Techniques Branch and the Laboratory Directed Research and Development program of the Pacific Northwest National Laboratory (PNNL) as part of the support for the Environmental Molecular Sciences Laboratory (EMSL) project. Funding for N.F. and K.K. was facilitated by Associated Western Universities, Northwest Division. PNNL is operated for the U.S. Department of Energy by Battelle Memorial Institute under Contract No. DE-AC06-76RLO 1830. T.A. expresses his gratitude to Professor Jeanne Small for contructive review and comments on this manuscript. Jerry Posakony and Oleg Puchenokov for the invaluable discussions regarding the properties of ultrasonic transducers. Professor Silvia Braslavski for insightful discussions regarding deconvolution of acoustic waveforms, and Professors Dick Caldwell and Lynn Melton for sharing their analysis program C2NLIN.

[1] S. E. Braslavsky and G. E. Heibel, Chem. Rev. **92**, 1381–1410 (1992).
[2] P. R. Crippa, A. Vecli, and C. Viappiani, J. Photochem. Photobiol., B **24**, 3 (1994).
[3] K. J. Peters, Angew. Chem. Int. Ed. Engl. **33**, 294 (1994).
[4] T. J. Burkey, M. Majewski, and D. Griller, J. Am. Chem. Soc. **108**, 2218 (1986).
[5] T. J. Burkey, Polyhedron **8**, 2681 (1989).
[6] I. R. Gould, J. E. Moser, B. Armitage, S. Farid, J. L. Goodman, and M. S. Herman, J. Am. Chem. Soc. **111**, 1917 (1989).
[7] R. R. Hung and J. J. Grabowski, J. Am. Chem. Soc. **114**, 351 (1992).
[8] L. J. J. Laarhoven and P. Mulder, J. Phys. Chem. B **101**, 73 (1997).
[9] J. A. LaVilla and J. L. Goodman, J. Am. Chem. Soc. **111**, 712 (1989).
[10] G.-L. Leu and T. J. Burkey, J. Coord. Chem. **34**, 87 (1995).
[11] P. A. MacFaul, D. D. M. Wayner, and K. U. Ingold, J. Org. Chem. **62**, 3414 (1997).
[12] T. Ni, R. A. Caldwell, and L. A. Melton, J. Am. Chem. Soc. **111**, 457 (1989).
[13] E. F. Walsh, V. K. Popov, M. W. George, and M. Poliakoff, J. Phys. Chem. **99**, 12 016 (1995).
[14] D. D. M. Wayner, E. Lusztyk, D. Page, K. U. Ingold, P. Mulder, L. J. J. Laarhoven, and H. S. Aldrich, J. Am. Chem. Soc. **117**, 8737 (1995).
[15] X. Song and J. F. Endicott, Chin. Phys. Lasers **204**, 400 (1993).
[16] J. E. Rudzki, J. L. Goodman, and K. S. Peters, J. Am. Chem. Soc. **107**, 7849 (1985).
[17] S. E. Braslavsky and K. Heihoff, in *Handbook of Organic Photochemistry*, Vol. 1, edited by J. C. Scaiano (Chemical Rubber, Boca Raton, 1989), pp. 327–355.
[18] L. J. Rothberg, J. D. Simon, M. Bernstein, and K. S. Peters, J. Am. Chem. Soc. **105**, 3464 (1983).
[19] M. Terazima and T. Azumi, Bull. Chem. Soc. Jpn. **63**, 741 (1990).
[20] L. A. Melton, T. Ni, and L. Qingzheng, Rev. Sci. Instrum. **60**, 3217 (1989).
[21] L. G. Arnaut, R. A. Caldwell, J. E. Elbert, and L. A. Melton, Rev. Sci. Instrum. **63**, 5381 (1992).
[22] O. V. Puchenkov and S. Malkin, Rev. Sci. Instrum. **67**, 672 (1996).
[23] O. V. Puchenkov, Biophys. Chem. **56**, 241 (1995).
[24] G. G. Yee and D. S. Kliger, J. Phys. Chem. **87**, 1887 (1983).
[25] J. I. Kim, G. Buckau, E. Bryant, and R. Klenze, Radiochim. Acta **48**, 135 (1989).
[26] R. Klenze, J. I. Kim, and H. Wimmer, Radiochim. Acta **52/53**, 97 (1991).
[27] D. A. Wruck, C. E. A. Palmer, and R. J. Silva, Radiochim. Acta (in press).
[28] J. I. Kim, R. Stumpe, and R. Klenze, *Topics in Current Chemistry, Laser-Induced Photoacoustic Spectroscopy for the Speciation of Transuranic Elements in Natural Aquatic Systems* (Springer, New York, 1990), Vol. 157, pp. 128–183.
[29] D. A. Schurig, G. L. Klunder, M. A. Shannon, and R. E. Russo, Rev. Sci. Instrum. **64**, 363 (1993).
[30] J. Feitelson and D. C. Mauzerall, J. Phys. Chem. **97**, 8410 (1993).
[31] J. Feitelson and D. Mauzerall, J. Phys. Chem. **100**, 7698 (1995).
[32] For a cylindrical source the amplitude of the acoustic wave decreases inversely with distance between the excitation source and detector.
[33] T. Q. Ni and L. A. Melton, J. Photochem. Photobiol. A **67**, 167 (1992).
[34] L. G. Arnaut and R. A. Caldwell, J. Photochem. Photobiol. A **65**, 15 (1992).
[35] From Snell's law $\sin \Theta_c = (n_1/n_2)$ where n_1 is the refractive index of the

Downloaded 06 May 2003 to 198.128.86.151. Redistribution subject to AIP license or copyright, see http://ojps.aip.org/rsio/rsicr.jsp

prism and n_2 is the refractive index of the rarer medium, either air or solvent.

[36] J. R. Small, L. J. Libertini, J. F. Heissenbuttel, J. T. Daniels, M. D. Eide, B. W. Tillman, K. L. Mrakovcich, E. W. Small, and R. D. Smith, *Proceedings of Time-Resolved Laser Spectroscopy in Biochemistry IV* (SPIE, Bellingham, WA, 1994), pp. 21–224.

[37] J. R. Small, L. J. Libertini, and E. W. Small, Biophys. Chem. **42**, 29 (1992).

[38] It is critical to have the reference and sample solution at the same temperature because the velocity of sound is highly temperature dependent a nanosecond time scale.

[39] H. M. Lai and K. Young, J. Acoust. Soc. Am. **72**, 2000–2006 (1982).

[40] Caldwell, Ref. 21 suggested the term *solvent quality factor* to compare the relative PA signal in one solvent to another.

[41] J. A. Riddick and W. B. Bunger, *Organic Solvents: Physical Properties and Methods of Purification*, 3rd ed. (Interscience, New York, 1970).

[42] Weast, *Handbook of Chemistry and Physics*, 63rd ed. (Chemical Rubber, Boca Raton, 1982).

[43] G. Allen, G. Gee, and G. J. Wilson, Polymer **1**, 456 (1960).

[44] Edo Corporation, Piezoelectric Ceramics, Salt Lake City, UT.

[45] Valpey–Fisher Corporation, The Users Guide to Ultrasound Products, Hopkinton, MA.

[46] G. S. Kino, *Acoustic Waves: Devices, Imaging, and Analog Signal Processing* (Prentice–Hall, Englewood Cliffs, NJ, 1987).

[47] M. G. Silk, *Ultrasonic Transducers for Nondestructive Testing* (Hilger, London, 1984).

[48] R. C. Smith and K. S. Baker, Appl. Opt. **20**, 117 (1981).

[49] From the experimental conditions (energy density 100 nJ μL) shown in Fig. 4, with $H_{th} \sim 1\ \mu$J, excitation volume $(V_0) \sim 10\ \mu$L. This yields a signal three times the electrostriction background, therefore absorption of 50 nJ/μL will still provide a signal greater than background.

[50] K. Heihoff and S. E. Bravslavsky, Chin. Phys. Lasers **131**, 183 (1986).

[51] S. Hu, G. J. Farrell, C. Cook, R. Johnston, and T. J. Burkey, Organometallics **13**, 4127 (1994).

[52] S. K. Nayak, J. Am. Chem. Soc. **115**, 6391 (1993).

[53] H. Sbizuka and H. Obuchi, J. Phys. Chem. **86**, 1297 (1982).

[54] H. Paul, R. D. Small, Jr., and J. C. Scaiano, J. Am. Chem. Soc. **100**, 4520 (1978).

Downloaded 06 May 2003 to 198.128.86.151. Redistribution subject to AIP license or copyright, see http://ojps.aip.org/rsio/rsicr.jsp